RESEARCH PAPER

Sea level pressure response to the specification of eddy-resolving sea surface temperature in simulations of Australian east coast lows

Christopher R. S. Chambers[1,2,3*], Gary B. Brassington[2], Jinyu Sheng[1], Ian Simmonds[3] and Kevin Walsh[3]

[1] Department of Oceanography, Dalhousie University, 1355 Oxford St., PO Box 15000, Halifax, Nova Scotia, Canada B3H 4R2

[2] Centre for Australian Weather and Climate Research, Bureau of Meteorology, 16, 300 Elizabeth Street, Sydney, NSW 2000, Australia

[3] School of Earth Sciences, University of Melbourne 3010, Victoria, Australia

Abstract: Four east coast lows (ECLs) were simulated with the Weather Research and Forecast model to investigate the influence of the sea surface temperature (SST) distribution on the sea level pressure (SLP). Each ECL was simulated with two different SST datasets: the Bluelink SST field and NCEP skin temperature field. The former resolved eddies in the East Australian Current while the latter did not. The simulated SLP fields in the eddy-resolving SST runs were compared with those in the non-eddy-resolving SST runs. On time-scales of about 48 hours, higher SSTs were associated with lower SLPs. The spatial scale of the SLP response was similar to that of the ocean eddies, indicative of the rapidity and robustness of the response given the rapidly evolving conditions within the storms. On shorter time-scales, the SLP response to SST change can become substantially larger. The largest reductions in SLP in the eddy-resolving SST runs were associated with regions of deep atmospheric convection that warm the tropospheric column. These areas were shown to be related to the SST distribution with the greatest SLP reductions associated with convection over strong SST gradient regions. The landfall of a damaging convective mesoscale low pressure system on 8 June 2007 was also investigated. It was found that a region of strong SST gradients on the southern flank of a large warm ocean eddy was associated with lower pressures at the time of formation of this meso-low. In addition, the only case that simulated the low pressure at the correct time (albeit at not quite the correct location) was the eddy-resolved SST run. It was hypothesized that the development of this meso-low that impacted the coast around Newcastle, was enhanced because of the eddy-scale SST distribution at the time.

Keywords: Pressure, Australia, temperature, sea, cyclone

*Correspondence to: Christopher R S Chambers,700 Collins St, Docklands, VIC 3008, Australia; Email: c.chambers@bom.gov.au

Received: November 7, 2015; **Accepted:** December 18, 2015; **Published Online:** February 26, 2016

Citation: Chambers C R S, Brassington G B and Sheng J *et al.* (2016). Sea level pressure response to the specification of eddy-resolving sea surface temperature in simulations of Australian East Coast lows. *Satellite Oceanography and Meteorology*, vol.1(1): x–x. http://dx.doi.org/10.18063/SOM.2016.01.001

1. Introduction

Surface winds are closely associated with the air pressure distribution in the lower troposphere. Local topographic features can change the pressure distribution and also change the winds, leading to regions of much stronger surface winds. Over the ocean, the air pressure distribution is also affected by the sea surface temperature (SST). Except for tornadoes, the lowest sea level pressure (SLP) on the Earth occurs over the warm oceans in tropical cyclones (TCs). Under favorable atmospheric and oceanic conditions, the heat and moisture fluxes from the ocean's surface provides the energy for the development of an atmospheric convective-vortex positive feedback (Charney and Eliassen, 1964; Emanuel, 1986) that may continue until the TC reaches its maximum potential intensity (MPI and Miller, 1958; Emanuel, 1988) or a somewhat greater intensity (Persing and Montgomery, 2003), provided that the intensification of the storm is not inhibited by unfavorable atmospheric conditions such as strong vertical wind shear. Observations showed that the MPI increases rapidly with increasing of SSTs. On smaller scales in deep convection within developing tropical cyclones, lower-tropospheric rotation (or the potential for rotation in the form of increased potential vorticity) can increase due to vortex stretching and/or mid-level latent heating (e.g., Hendricks, Montgomery and Davis, 2004). Rotation can also be induced by deep vertical convection due to updraft-forced tilting of vertical wind shear induced vorticity (Browning and Landry, 1963), for example, in supercells. The flux of heat and moisture from the ocean's surface can impact all of these phenomena and consequently indirectly impact the SLP from the TC scale down to the thunderstorm scale.

In addition to these convective-vortex processes, SSTs and their gradients have long been suspected of affecting large-scale, mid-latitude synoptic cyclogenesis in the atmosphere (Pope, 1968). Sanders and Gyakum (1980) found that explosive development of extratropical cyclones occur preferentially near regions with strongest gradients in SST. Roebber (1984) used a climatology of explosive cyclones to show that the position of the midpoint of the period of maximum 24-hour deepening most often corresponded with regions of strong mean SST gradients. Cione *et al.* (1993), Giordani and Caniaux (2001), Lim and Simmonds (2002), and Jacobs *et al.* (2008) demonstrated that strong lower-tropospheric temperature gradients in both the Northern and Southern Hemispheres facilitated storm formation and intensification.

Both convective-vortex and baroclinic instability processes have been suggested to be considered in this study as it is important in the development of the Australian east coast lows (ECLs, Holland, Lynch and Leslie, 1987). These intense low pressure weather systems can develop rapidly off the Australian east coast where the warm East Australian Current (EAC) flows southward. ECLs have a large range in size from 50 km to 1000 km, and can last for a few hours to several days. There are about 10 ECLs on average per year and they preferentially occur in the autumn and winter months. ECLs generally develop within a lower-tropospheric trough east of, or under, a mid-tropospheric cold core trough or cyclone. Along with low- level baroclinicity, strong upper-level forcing has been shown to be a very important feature associated with rapid deepening of extratropical cyclones (Jacobs, Lackmann and Raman, 2005). ECLs are responsible for significant weather and ocean related damage in the coastal regions of east Australia (Bridgman, 1986; Holland, Lynch and Leslie, 1987; Mills, Webb, Davidson *et al.*, 2010; Pepler, Di Luca, Ji *et al.*, 2015). Simulations suggested that heavy coastal rainfall during a particularly damaging ECL in 2007 was increased because of the presence of a large warm ocean eddy in the EAC (Chambers, Brassington, Simmonds *et al.*, 2014). The work presented here builds on the investigation of Chambers *et al.* (2014) with the focus being on the SLP sensitivity to SST, as well as extending the analysis to include three additional ECL cases.

The EAC sheds anticyclonic eddies of the order of 250 km diameter near 35°S. These eddies are shed more frequently and in a more clearly defined region than in other intense western boundary current systems such as the Gulf Stream (Hamon, 1965). As warm eddies or current filaments move southward, they enter a progressively cooler ocean environment. As a consequence, regions of large SST gradients develop off the east coast as these two water masses collide (Andrews, 1979). The sensitivity of Australian cut-off lows (defined as a closed cyclonic circulation at 500 hPa and precursors to the formation of ECLs) to increases in SST was examined numerically by McInnes *et al.* (1992). They found that raising SSTs by 2 to 3°C in simulations over southeast Australia caused decreases in SLP of 1 to 7 hPa.

SST gradients have been found to impact the ma-

rine atmospheric boundary layer. In regions of large SST gradients, a strong positive correlation between SST and surface wind speed perturbations exists (see review by Small, deSzoeke, Xie *et al.*, 2008). As a consequence, there is a tendency for convergence to occur as air flows from warm to cool SSTs. This convergence has also been associated with deep convection and Kuwano-Yoshida *et al.* (2010) found convective precipitation to be sensitive to SST gradients along the Gulf Stream. In addition to surface convergence over regions of large SST gradients, satellite scatterometer observations over the Gulf Stream have shown that surface winds rotate counterclockwise as winds blow from warm to cool water (Park, Cornillon and Codiga, 2006). A 4° to 8° wind direction response occurs for typical SST gradients associated with the major western boundary currents (O'Neill, Chelton and Esbensen, 2010a). In the Southern Hemisphere the situation is reversed and winds from warm to cool SSTs turn clockwise (that is, cyclonically).

The main objectives of this study were to (a) improve our understanding of the local SLP response to the SST from day to hourly time scales and (b) establish the role that the SST distribution plays in the development of observed damaging storm features in ECLs. The Weather Research and Forecast (WRF) model was used in numerical experiments of four ECLs to examine the sensitivity to SST fields. The different SST datasets used in this study have different spatial resolutions, which lead to differences in the eddy-scale SST distributions and spatial gradients. O'Neill *et al.* (2010b) showed, based on a month-long average of perturbation SLP from a WRF model simulation over the Aghulas Return Current, that low pressure perturbations form on the downwind side of warm SST perturbations (their Figure 2). For the ECL simulations presented here the time-scales were on the order of hours and days, considerably shorter than the time-scale of about 1 month considered in O'Neill *et al.* (2010b), so considerable interest will be centered on the short-term “spin-up” of the SLP to changes in the SST. Furthermore, our simulations covered specific storm events to determine the characteristics of these relationships during occurrences of damaging weather. The structure of this paper is as follows. The atmospheric circulation model and setup used in this study are described in section 2. Model results are presented in section 3. Summary and discussion are presented in section 4.

2. Method

The ECL simulations were conducted using version 3.3.1 of the WRF model (Skamarock, Klemp and Dudhia *et al.*, 2005) with a two-level nested-grid configuration, in which a fine-resolution (3 km) inner model domain was nested inside a coarse-resolution (15 km) outer domain (Figure 1). Both the outer and inner domains were on a Lambert conformal grid. The outer domain was 221 by 171 grid points (3315 km by 2565 km) and the inner domain was 301 by 261 grid points (903 km by 783 km). The inner domain was centered on the region of ECL development (as discussed in detail in section 3). There were 55 terrain-following hydrostatic-pressure levels used in the vertical with a model top at 30 hPa. This study also used the Final Analysis (FNL) atmospheric data with a horizontal resolution of 1° produced by the National Centers for Environmental Prediction (NCEP) (Global Climate and Weather Modeling Branch, 2003) for both boundary conditions and initialization.

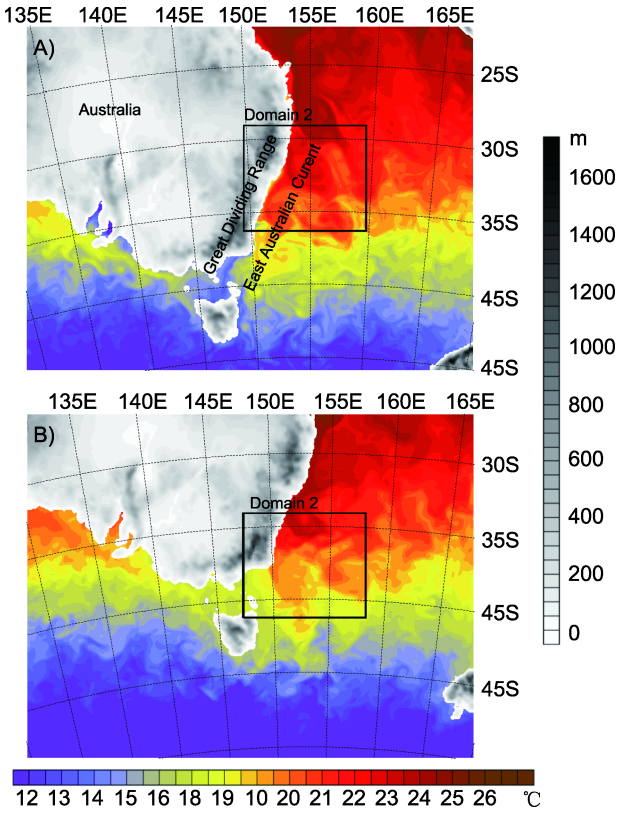

Figure 1: 15 km (whole map) and 3 km (the area marked by the black box) resolution domains with terrain height (m) for (A) simulations in 2007 and (B) simulations in 2012. Color image over the ocean represents (A) BRAN SST for 1200 UTC 6 June 2007 and (B) OceanMAPS SST for 1200 UTC 23 April 2012

The nested-grid model used the microphysics scheme suggested by Thompson *et al*. (2004), which contained six water classes (water vapor, cloud water, rain, snow, graupel, and cloud ice). The model also used the Yonsei University planetary boundary layer parameterization with the Monin-Obukhov surface layer scheme (Hong, Noh and Dudhia, 2006), the short wave radiation scheme suggested by Dudhia (1989), and the Rapid Radiative Transfer Model (RRTM) for long wave radiation with six molecular species (Mlawer, Taubman, Taubman *et al*., 1997). The outer domain also used the Betts-Miller-Janjic cumulus scheme (Betts, 1986; Betts and Miller, 1986; Janjic, 1994).

The nested-grid model was used to simulate ECLs in four case studies: (a) 6-9 June 2007, (b) 15-17 June 2007, (c) 23-26 April 2012, and (d) 3-5 June 2012. Two numerical runs were conducted for each case. The model setup and parameterizations in each pairs of runs were the same except for different SST fields used as input (Table 1). The WRF model took 6-hourly SST fields in all of the eight model runs.

Three types of SST fields were used in this study. The first type was the SST field taken from the Bluelink ReANalysis (BRAN) (Schiller, Oke, Brassington *et al*., 2008). BRAN is the daily output of an eddy-resolving ocean model simulation using the Modular Ocean Model (MOM) (Griffies, Harrison and Pacanowski, 2004) which is constrained through the data assimilation of altimetry, remote sensing SST and *in situ* profiles using the Bluelink Ocean Data Assimilation System (BODAS) (Oke, Brassington, Griffin *et al*., 2008). Over an Australian-centred region (90°E-180°E, 75°S-16°N), the BRAN fields have a resolution of 0.1 degrees and the nested-grid outer and inner model domains lie entirely within this region. The daily BRAN fields were interpolated to 6-hourly fields to be consistent with the atmospheric initial conditions.

The second type is the SST field produced by version 2 of the Bluelink Ocean Model, Analysis and Prediction System (OceanMAPS) (Brassington, Freeman, Huang *et al.*, 2012). OceanMAPS uses a global ocean model based on version 4 of the Modular Ocean Model (MOM4) with data assimilation of BODAS observations. Since both the BRAN and the OceanMAPS utilized the MOM, they produced subjectively similar SST features in the EAC, including the presence of mesoscale filaments and eddies, as shown in the left panels of Figure 2. Because of the availability of Bluelink reanalysis data, the BRAN SST fields were used in two runs of ECL simulations in 2007 (i.e., JUN07a_BN and JUN07b_BN), while the OceanMAPS SST fields were used in two runs of the ECL simulations in 2012 (i.e., APR12_OM and JUN12_OM).

The third type was the "skin temperature" field over the ocean from the NCEP FNL Operational Global Analysis data with a horizontal resolution of 1 degree derived from the Global Data Assimilation System (GDAS). The skin temperature field did not resolve eddies in the EAC, as was evident in the right panels of Figure 2. It should be noted, however, that large-scale features in the Bluelink SSTs and skin temperatures were very similar, with generally warmer surface waters to the north and colder waters to the south off the east coast of Australia. Table 2 listed area-means of the 48-hour averaged SSTs calculated from the Bluelink SSTs and skin temperatures during the period between 12 and 60 hours from the simulation initialization over the region of 150°E-158°E and 34°S-41°S for cases JUN07a and JUN07b in 2007 and over the region 151°E-159°E and 29°S-36°S for cases APR12 and JUN12 in 2012. Both the Bluelink SSTs and skin temperatures have very similar area-mean values in the four cases, with a mean difference (Bluelink-skin) across the four cases of –0.09°C and a mean magnitude difference of 0.29°C.

Table 1: Names of the four cases, the simulation period in each case, and the name and SST data used in each run

Case	Simulation Period	Run	Input SST Field
JUN07a	1200 UTC 6 to 0000 UTC 9 June 2007	JUN07a_BN	BRAN
		JUN07a_skin	NCEP skintemp
JUN07b	0000 UTC 15 to 1200 UTC 17 June 2007	JUN07b_BN	BRAN
		JUN07b_skin	NCEP skintemp
APR12	1200 UTC 23 to 0000 UTC 26 April 2012	APR12_OM	OceanMAPS
		APR12_skin	NCEP skintemp
JUN12	0000 UTC 3 to 1200 UTC 5 June 2012	JUN12_OM	OceanMAPS
		JUN12_skin	NCEP skintemp

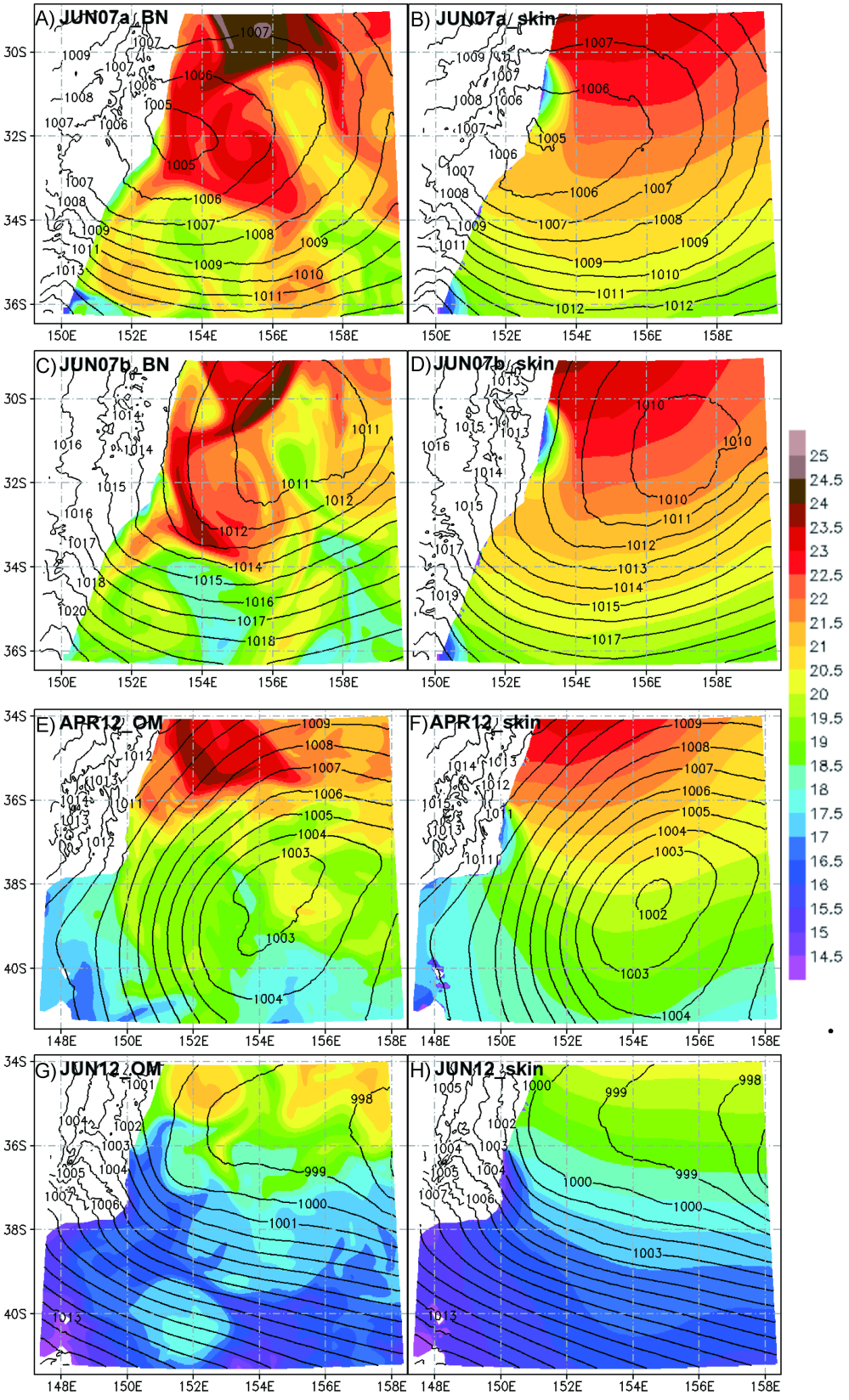

Figure 2: The time-mean fields (colors, °C) of Bluelink SSTs (left) and Skin temperatures (right) over the 48-hour analyzed period in cases (A) JUN07a, (B) JUN07b, (C) APR12 and (D) JUN12. Black contours represented the 48-hour time-mean sea level pressures (hPa) produced by the nested-grid inner model based on the WRF in each run for the analysis periods (refer to Table 1).

Table 2: Area means of the 48-hour averaged Bluelink SST and skin temperature over the area of 150°E-158°E and 34°S-41°S for cases JUN07a and JUN07b, and over the area 151°E-159°E and 29°S-36°S for cases APR12 and JUN12

Case Name	Bluelink SST	Skin Temperature
JUN07a	21.58	21.35
JUN07b	20.63	21.26
APR12	20.09	20.22
JUN12	17.91	17.75

To further examine the advantage of the Bluelink SST field, the time-mean (48-hour-averaged) differences between Bluelink SSTs and skin temperatures over the inner model domain were calculated and presented in Figure 3 for four cases. Since the skin temperature fields were large-scale and spatially smooth in comparison to the Bluelink fields, large (positive or negative) differences shown in Figure 3 were mainly associated with the meso-scale features in the Bluelink SST fields. The Bluelink SST field shave areas of higher temperatures over the warm eddies (e.g., region I in Figure 3a) as well as regions of cooler temperatures, for example where a cold tongue of water is resolved (e.g., region II). The JUN07b case (Figure 3b) was notable for the dominance of cooler SSTs in the Bluelink than in the Skin simulations. The Bluelink dataset exhibited stronger SST gradients with more complicated patterns than the Skin dataset. It follows that the strong gradients in the SST differences corresponded mainly to strong gradients in the Bluelink SST data.

For ease of reference, simulations using the BRAN

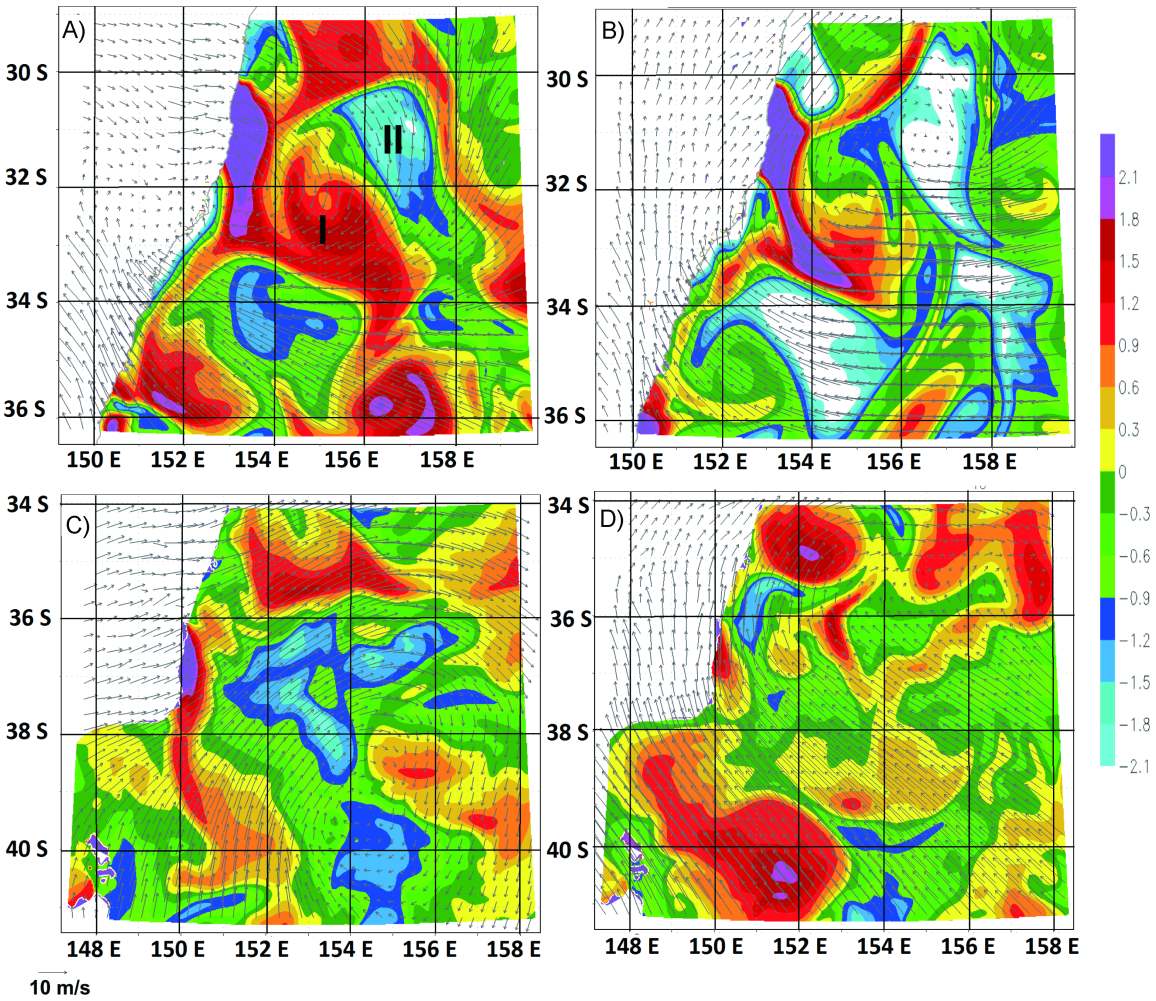

Figure 3: Time-mean differences in the sea surface temperature (color image, °C) between the Bluelink and Skin simulations over the 48-hour analyzed period in cases (A) JUN07a, (B) JUN07b, (C) APR12 and (D) JUN12. Overlaid were the 48-hour averaged 10 m wind vectors for the BN/OM cases where 10 m s^{-1} corresponded to the arrow length indicated in the bottom left. The locations 'I' and 'II' in (A) were example areas where the Bluelink simulation had warmer and cooler SSTs respectively.

or OceanMAPS SST fields are referred to as the "Bluelink" simulations (or runs), and those using the skin temperature field are referred to as the "Skin" simulations (or runs). The WRF nested-grid model was initialized from the NCEP atmospheric data at (a) 1200 UTC 6 June 2007, (b) 0000 UTC 15 June 2007, (c) 1200 UTC 23 April 2012, and (d) 0000 UTC 3 June 2012 respectively for cases JUN07a, JUN07b, APR12, and JUN12 (Table 1). The nested-grid model was integrated for 60 hours from the initialization in each model run with the NCEP atmospheric data updated every 6 hours at the boundary of the outer nest. Model results for the first 12 hours after the initialization were considered as model spin-up. Model results during the 48-hour period after the spin-up in each run were examined in this study.

3. Results

In order to place our results in context, we first examined the SLP analyses made by the National Meteorological and Oceanographic Centre of the Australian Bureau of Meteorology (NMOC-ABOM) during the four case studies periods. Figure 4 presented these analyses for the four ECL cases at the time of lowest analyzed SLP. It indicated that the ECL centers were positioned to the east of Newcastle for cases JUN07a and JUN07b in 2007 (Figure 4a and b) and located near the southeast corner of Australia for cases APR12 and JUN12 in 2012 (Figures 4c and d). This was the main reason why the region covered by the inner model domain for two ECL cases in 2007 (Figure 1a) differed from the region for two ECL cases in 2012 (Figure 1b). The lowest SLP in the NMOC-ABOM analyses of four ECL cases was 986 hPa, which occurred on 4 June 2012 (Figure 4d).

In comparison to the analyzed data shown in Figure 4, the nested inner domain reproduced reasonably well for the large-scale features of SLP in terms of the structure and the center position of the ECLs for the four study cases. The time-mean SLP averaged from model results during the 48-hour period (after the model spin-up of 12 hours) were presented in

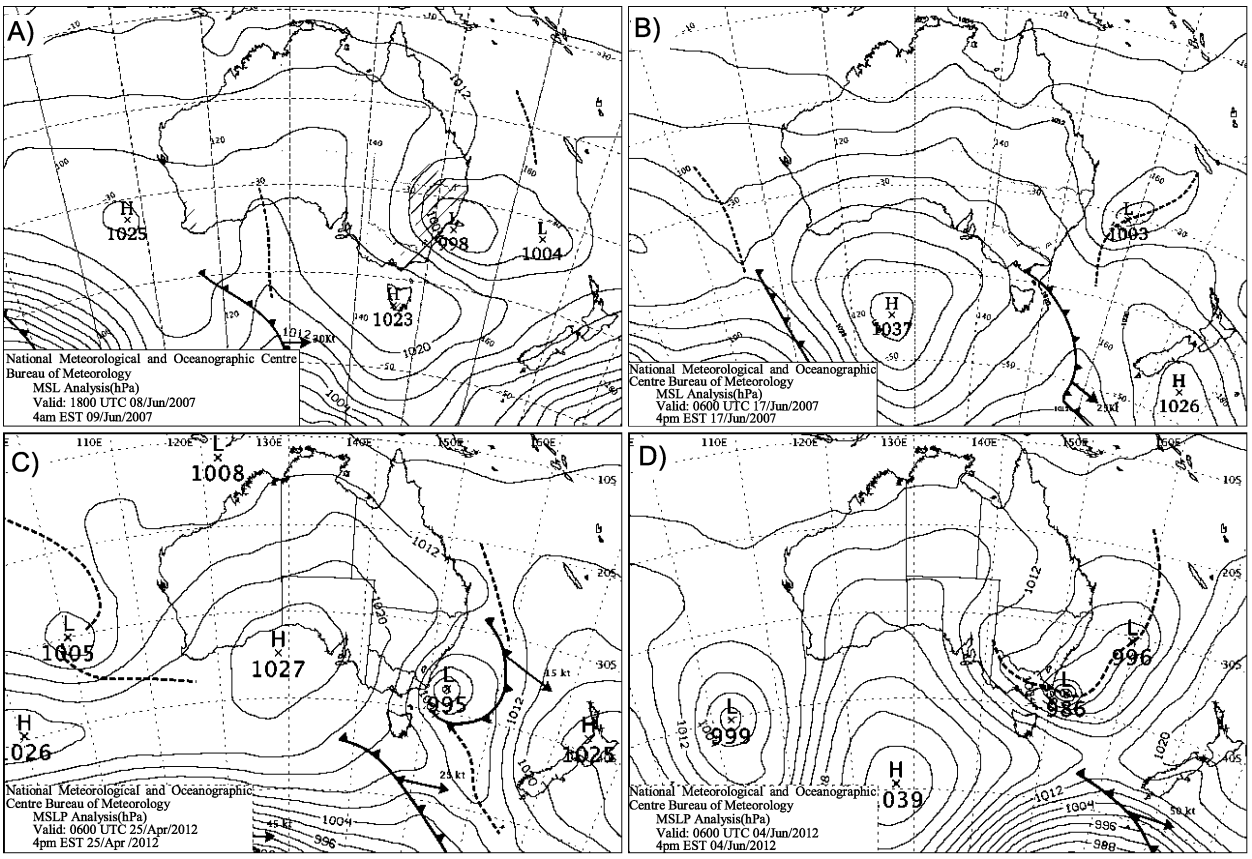

Figure 4: Sea level pressure analyses from the National Meteorological and Oceanographic Centre of the Australian Bureau of Meteorology (NMOC-ABOM) for the time of lowest analyzed sea level pressure for each case; A) 1800 UTC 8 June 2007, B) 0600 UTC 17 June 2007, C) 0600 UTC 25 April 2012, and D) 0600 UTC 4 June 2012.

Figure 2. The 48-hourly time-mean SLP fields in both the Bluelink and Skin simulations had very similar large-scale patterns. The time-mean SLP simulated over the inner domain had the minimum central pressure located approximately at 153.0°E, 32.0°S, over coastal waters off Newcastle in runs JUN07a_BN and JUN07a_skin (Figures 2a and b), and approximately at 157°E, 31°S in the shelf waters to the east of Newcastle in runs JUN07b_BN and JUN07b_skin (Figures 2c and d). The 48-hour mean minimum SLP produced on the inner domain was located approximately at (154.5°E, 38.3°S) in the shelf waters to the southeast of Australia in runs APR12_OM and APR12_skin (Figures 2e and f). For JUN12_OM and JUN12_ skin, by comparison, the 48-hour mean SLP produced by the inner model did not have a well-defined low pressure center (Figures 2g and f), mainly due to the high translational speed of the storm during this 48-hour period.

There were clear differences, however, between the Bluelink and Skin simulations in the 48-hourly time-mean SLP averages. In run JUN07a_BN for example, there was a larger region enclosed by the 1005 hPa contour around the low pressure center in comparison with the counterpart in run JUN07a_skin, which was indicative of a slightly lower central pressure in the Bluelink simulation than the Skin simulation for case JUN07a. For case JUN07b, the minimum time-mean SLP in JUN07b_skin was lower than the value in JUN07b_BN (Figures 2c and d). Run APR12_skin also had a lower minimum time-mean SLP than APR12_ OM. The 1003 hPa closed isobar in APR12_OM had a kink fold on its southwest side that was absent in APR12_ skin. JUN12_OM had a notable bulge in the 1000 hPa contour near (151°E, 37°S) that was absent in JUN12_ skin. This bulge occurred over a small warm eddy at this location apparent in the 48-hour-averaged SSTs. JUN12_OM also had a 999 hPa isobar that expanded further to the west (152.5°E) than in JUN12_skin (153°E).

Figure 5 presented time series of minimum SLPs calculated from the WRF model results (hourly) and from the NMOC-ABOM analyzed data (6-hourly) over the inner model domain for the four ECL cases. The minimum SLPs in both Bluelink and Skin simulations had significant temporal variability which was similar to the analyzed time series in cases JUN07a, JUN07b and JUN12. For case APR12, the minimum SLPs produced by the WRF model were more than 7 hPa lower than the values suggested by the ABOM analyses. It was speculated that this difference was due to a lack of observation over the Tasman Sea leading to a poor analysis rather than a large model deficiency. This speculation was supported by the well-defined storm structure revealed in the relevant satellite image, which suggested a lower pressure than the analyzed case for APR12.

Figure 5a verified that the minimum SLP in JUN07a_BN was generally lower than the counterpart in JUN07a_skin from 0400 UTC 7 June to 1800 UTC 8 June. After 1700 UTC 8 June, the minimum SLP in JUN07a_skin was about 3 to 4 hPa lower than its counterpart in JUN07a_BN. JUN07a_BN developed a 995 hPa low at 1230 UTC 8 June that made landfall at 1330 UTC as a 998 hPa cyclone. This occurred at a similar time to the most intense observed land falling low at 1430 UTC 8 June with a minimum SLP of 995 hPa (Mills, Lackmann, Davidson *et al.*, 2010, their Figure 5). In contrast, JUN07a_skin developed a less distinct low around this time that reached a minimum SLP of 998 hPa. Model results in JUN07b_BN and JUN07b_skin had similar minimum SLP until 1400 UTC 16 June. After that time JUN07b_skin deepened rapidly followed by JUN07_BN four hours later. For the final 10 hours of the simulation JUN07b_skin had a minimum SLP approximately 1 hPa lower than JUN07b_BN.

The model results in cases APR12 and JUN12 in 2012 had minimum SLPs lower than two ECL cases in 2007. APR12_OM developed a deeper pressure than APR12_skin, despite APR12_skin having a slightly higher time-mean SST in the region (Table 2). Both of the JUN12 cases had similar minimum SLPs up to 1000 UTC 4 June, after which JUN12_skin tended to have up to 2 hPa lower minimum SLP than JUN12_ OM. As indicated in Figure 5c, the minimum SLP over the inner model domain after 1400 UTC 4 June was actually associated with a secondary offshore low pressure, and not the weakening smaller land falling low pressure that caused the damage on the coast.

In order to further examine the effect of the SST on the SLP, the 48-hourly time-mean differences between the Bluelink and Skin runs in each ECL case were calculated and presented in Figure 6, with the 48-hourly time- mean SST differences and 10-m wind fields shown in Figure 3. Figure 6a indicated that the Bluelink run in case JUN07a had higher time-mean pressures centered approximately at (157.2°E, 32.7°S) and lower pressures centered approximately at (153.5°E, 31.5°S), than the skin temperature run. The

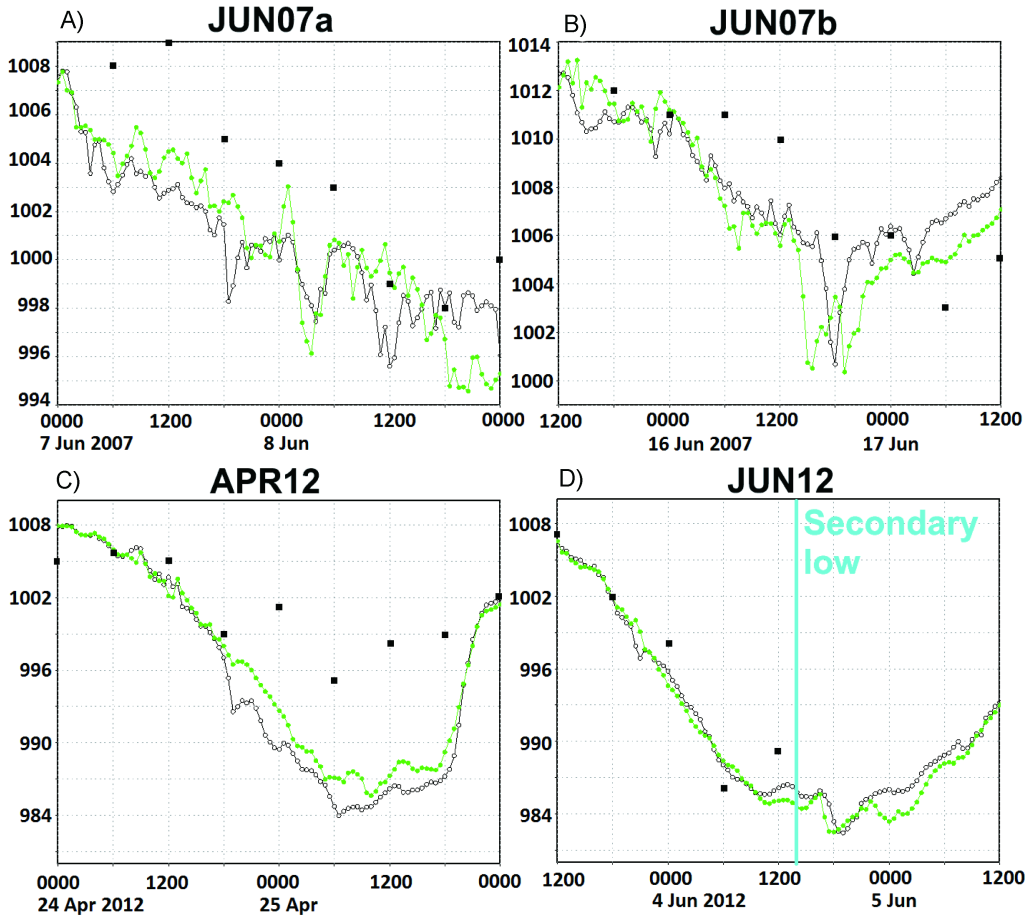

Figure 5: Time series of minimum sea level pressures over the inner model domain over the 48-hour period calculated from Bluelink (open circles) and Skin (closed green circles) hourly simulations and the NMOC-ABOM analyzed 6 hourly sea level pressures (black squares).

48-hourly time-mean winds shown in Figure 3a indicated that the higher pressure region was, on the average, the downwind region of cooler SSTs, while the lower pressure roughly spreads across the warmer SST region. Over other regions, the lower SLPs centered approximately at (156.0°E, 35.5°S), (156.5°E, 29.5°S) and (151.0°E, 34.0°S) respectively occurred in the downwind regions of warmer SSTs in JUN07a_BN (Figure 6a).

Figure 6b showed that there were generally higher pressures in JUN07b_BN than JUN07b_skin over the inner model domain. JUN07b_BN had a larger area of cooler temperatures than any of the other simulations and the magnitude of the cooling was also larger than the other cases. These cooler SSTs were associated with a rise in the SLP across the inner model domain by over 1 hPa across a broad area in the southern and eastern parts of the domain. There were three distinct areas of maximum pressure increases over these regions, which corresponded to the three regions of negative SST differences in Figure 3, while the smallest pressure rise occurred in the downwind region of a positive SST difference around 154.0°E, 31.0°S.

The 48-hourly time-mean SLP and SST differences shown in Figure 6c and d for cases APR12 and JUN12 demonstrated additional SLP responses to SST changes. There was a pronounced dipole of pressure perturbations over the southern part of the inner model domain (Figure 6c), reflecting the lower pressures to the west of 153°E and higher pressures to the east in the Bluelink run (APR12_OM) than its counterparts in the Skin simulation (APR12_OM). Run APR12_OM had a storm with a lower central pressure and a tighter cyclonic circulation and the higher pressure gradient implied by the large gradient in pressure differences across the pressure dipole were a result of this difference in the storm structure. This phenomenon provided a complex example of pressure differences amplifying over time in response to differences in the SST distribution. In order to understand how this

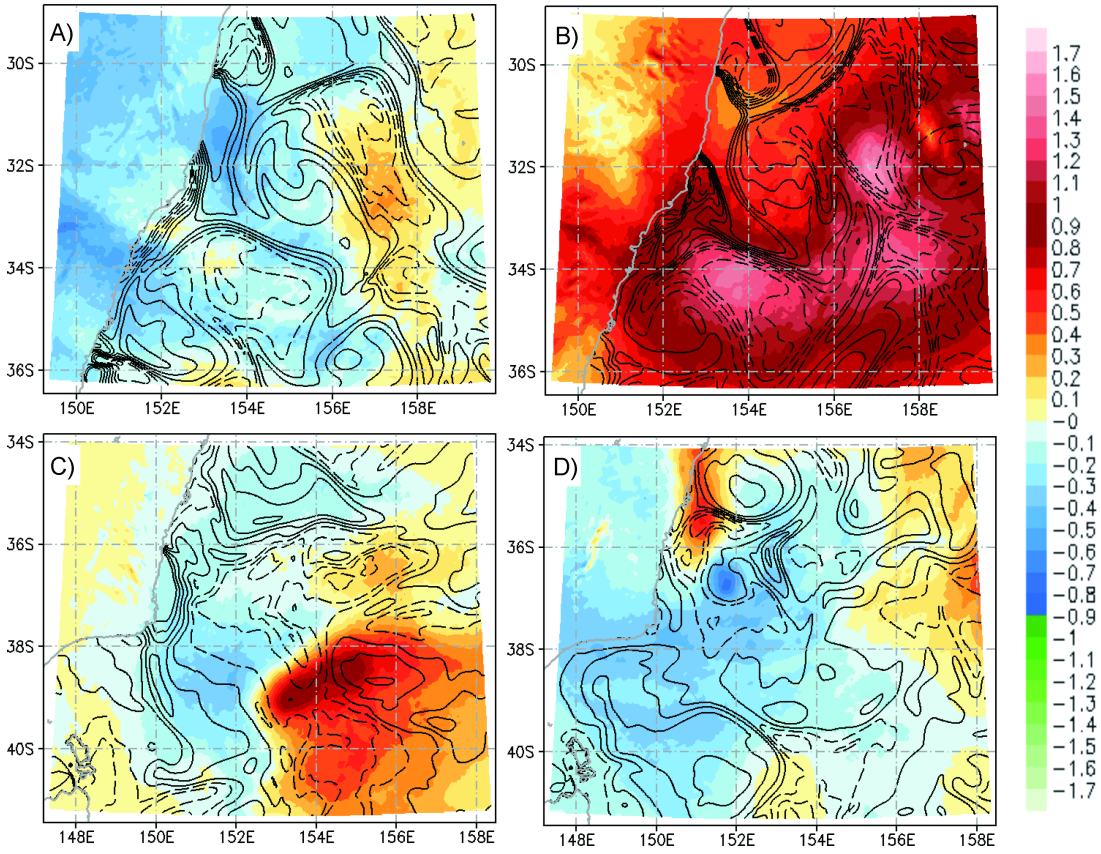

Figure 6: The 48-hourly time-mean differences in the sea level pressure (color image, hPa) between the Bluelink and Skin simulations in cases: (A) JUN07a, (B) JUN07b, (C) APR12_OM, and (D) JUN12. The time-mean differences in the sea surface temperature (contours) between the Bluelink and Skin simulations were overlaid for reference as contours (refer to Figure 3 for greater detail) with dashed line as negative at 0.5°C intervals.

phenomenon developed, an analysis focusing on the intensification phase of the storm was required.

Figure 7 presented 24-hourly time-mean differences in the SLP and SST between the Bluelink and Skin simulations during the first 24 hours of the 48-hour analyzed period for the four cases. This was the period during which the ECLs were developing and intensifying (Figure 5). Over this period, the 24-hourly time-mean local pressure differences of -0.9 hPa in JUN07a occurred over the warmer waters near (154°E, 32°S), but generally the warmer waters of the warm eddy, the pressure difference is about -0.5 hPa (Figure 7a). For JUN07b (Figure 7b) there was a generally similar pattern in the pressure differences to the 48-hourly time-mean with a notable difference being the negative pressure differences over the warmer SSTs around (154°E, 32°S). By comparison, the 48-hourly time-mean pressure differences were positive almost over the whole domain (Figure 6b).

Figure 7c demonstrated that the marked dipole in the sea level pressure difference present in Figure 6c had not developed during the first 24-hour period. Instead, a general weaker dipole existed that appeared strongly related to the SST differences. The lower pressures in the west developed over the warmer waters in this area while the higher pressures spread downwind of the cooler waters in the northerly flow during this period. This general pattern gets gradually amplified as the storm developed in the vicinity of this dipole.

By comparison, in case JUN12b, a signature of a dipole had already developed during the first 24-hour period over the northwest area close to the coast of the inner model domain. This dipole was an indication of a stronger pressure gradient on the western flank of the low in JUN12b_OM than its counterpart in JUN12_skin. In JUN12_OM cooler waters contrasted with warmer waters off shore approximately at 152°E, 36.5°S. The presence of the developing low pressure center in this area appeared to amplify the SLP response.

Figure 8 presented 24-hourly time-mean differences in the SLP and SST between the Bluelink and Skin

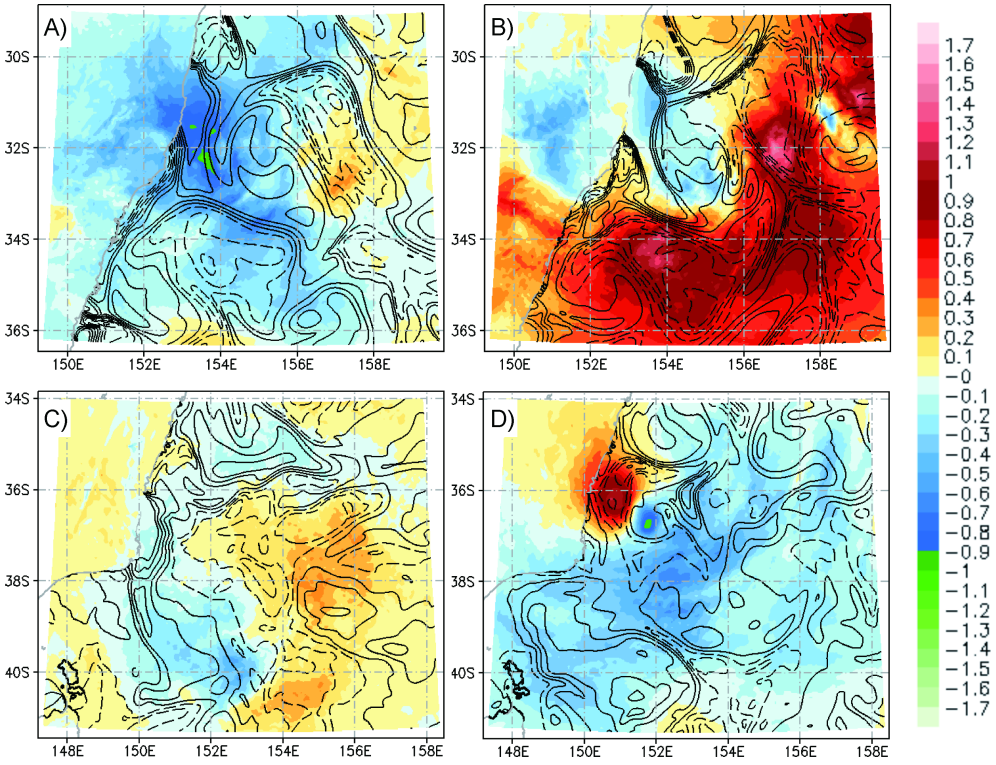

Figure 7: Time-mean differences in the sea surface pressure (color image, hPa) and sea surface temperature (contours, °C) for the first 24 hours of the 48-hour analysis period in the four cases. Otherwise as in Figure 6.

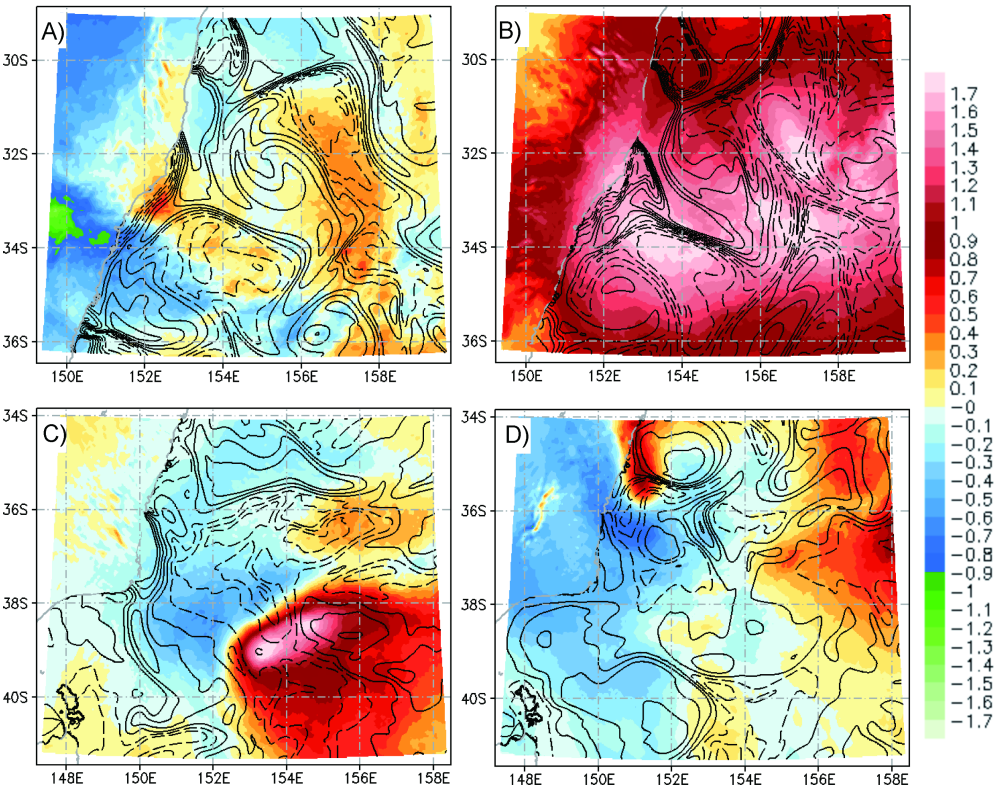

Figure 8: Time-mean differences in the sea surface pressure (color image, hPa) and sea surface temperature (contours, °C) for the second 24 hours of the 48-hour analysis period in the four cases. Otherwise as in Figure 6.

simulations during the second 24 hours of the 48-hour analyzed period for the four cases. The large negative SLP differences between JUN07a_BN and JUN07a_skin occurred over the southwest part of the inner model domain associated with a convective rainband and embedded mesoscale low pressure regions. By comparison, JUN07b_BN had higher 24-hourly time-mean SLPs than JUN07b_skin over the whole inner model domain (Figure 8b); where the Bluelink SSTs were significantly lower than the Skin temperatures in JUN07b case.

The model results in two ECL cases in 2012 exhibited a less clear relationship between the SLP and SST during the second 24-hour period (Figure 8c and d). A comparison of Figures 6c and 8c indicated that the dipole in the 48-hourly time meant that SLP differences were mainly due to the development of this feature in the second 24-hour period. This dipole was caused by a more compact low pressure system in APR12_OM. This was evidence that changing the SST did in fact change the structure of the entire storm in this case. The first 24-hour period JUN12 dipole seen in Figure 7d had shifted in position and orientation by the second 24-hour period (Figure 8d). During this latter period, the dipole was centered approximately at 151.0°E, 35.7°S with pressures higher to the north and lower to the south of the dipole. Interestingly, this dipole no longer has a strong direct connection with the distribution of SST difference. This was probably because changing the SST structure had caused a change in the structure of the low pressure system during the first 24-hour period and the translation of the storm by the second 24-hour period had shifted the locations of the SLP response. In fact all of the cases had a lower correlation between SLP difference and SST difference in the second 24-hour than the first 24-hour period. This indicated the SLP response to changing the SST can evolve rapidly and in a very complicated fashion, and suggested the impact of feedback processes.

The above analyses of model results demonstrated large temporal variability between the first and second 24-hour periods in the SLP response to the SSTs in the four ECL cases. As expected, the SLP response to the SST with shorter timescales and finer spatial scales will emerge from time-mean SLP and SST differences between Bluelink and Skin simulations averaged over periods shorter than 12 hours. As an example, Figure 9

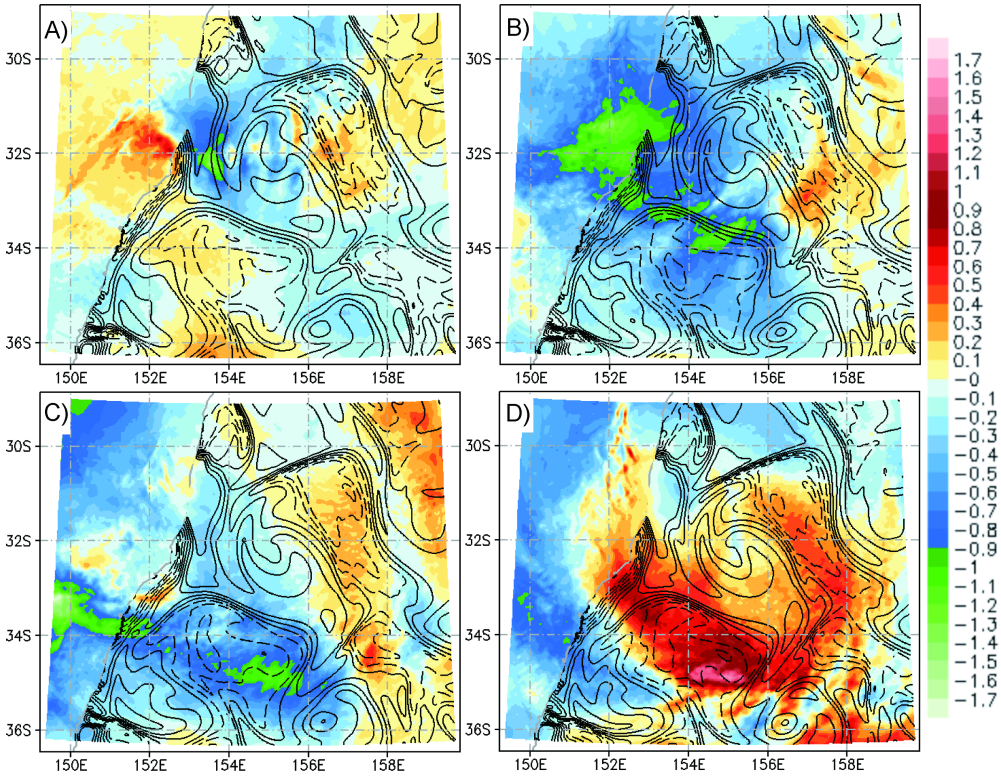

Figure 9: The 12-hourly time-mean differences in the sea level pressure (color image, hPa) and sea surface temperature (contours, °C) between the Bluelink and Skin simulations averaged over the period of (A) 0000 to 1200 7 June, (B) 1200 7 June to 0000 8 June, (C) 0000 to 1200 8 June, and (D) 1200 8 June to 0000 9 June in 2007. Otherwise as in Figure 6.

presented the 12-hourly time-mean SLP and SST differences between the Bluelink and Skin simulations for JUN07a. As discussed by Mills *et al.* (2010) and Chambers *et al.* (2014), the ECL in this case was associated with a southward propagating convective rainband that caused significant coastal damage near 33°S. The greatest pressure reductions in the 2nd and 3rd 12-hour periods (Figure 9b and c) were directly associated with this rainband. This meant that the effect of the introduction of Bluelink SSTs was to lower the SLP in the most damaging region of the storm. However the evolution of the SLP difference response is by no means collocated with regions of higher or lower SSTs. During the first 12-hour period, lower pressures did generally occur over the warmer SST regions. However, by the second 12-hour period the greatest pressure reductions were along the southern flank of the warm eddy (Figure 9b). This reduced SLP within the convective rainband remained as a signal in the 3rd 12-hour period even though by this time the band laid over lower SSTs in the Bluelink simulation (Figure 9c). By the final 12-hour period, the cooler SSTs appeared to impact the SLP with occurrence of higher pressures (Figure 9d).

Within the convective rainband, an intense mesoscale low pressure system was developed on 8 June 2007 (Mills, Webb, Davidson *et al.*, 2010). The radar reflectivity shown in the right panels of Figure 10 indicated that this meso-low approached the coast and made landfall between 1130 UTC and 1430 UTC 8 June. Coastal observations recorded a minimum pressure at landfall of 995 hPa (Mills, Webb, Davidson *et al.*, 2010). For a direct comparison, the corresponding model-derived radar reflectivity calculated from the Bluelink and Skin simulations was also presented in the middle and left panels of Figure 10. The horizontal scale was the same between the model fields and the observed radar plot. Since the simulated rainband was further south than observed by this time period, the model fields shifted 1 degree latitude south of the radar plot to center the plot on the rainband. A comparison of left and right panels of Figure 10 indicated that JUN07a_skin did not simulate well the distinct meso-low during this period. By comparison, JUN07a_BN did simulate a meso-low that reached a minimum SLP of 995 hPa by 1230 UTC 8 June. The meso-low in JUN07a_BN had a similar horizontal scale to the observed meso-low. Furthermore, the meso-low simulated in JUN07a_BN occurred over the region of reduced SLPs approximately at (152.5°E, 34°S) (Figure 9c), which suggested that this meso-low was associated with SST forced lowered SLP. It was hypothesized therefore, that the development of this meso-low as well as the severity of the thunderstorm band that impacted the coast around Newcastle was enhanced because of the eddy scale SST distribution at the time period.

4. Summary and Discussion

Four ECLs were simulated using the WRF model with a two-domain nested grid to investigate the influence of the sea surface temperature SST distribution on the SLP. Each ECL case was simulated with two different SST fields: Bluelink SST and NCEP skin temperature. The former resolved meso-scale SST features associated with EAC eddy while the latter did not. The fields of SLP, SST and 10-m wind produced by the nested-grid inner domain in the Bluelink and Skin runs were used to examine the effect of the SST on the SLP. At timescales of about 48 hours, warm SSTs were associated with lower sea level pressures. The scale of this response was on the same horizontal scale as the EAC eddies, which was indicative of the rapidity and robustness of the response, given the rapidly evolving conditions within the storms. On shorter time-scales, the SLP response to SST change can become substantially larger. The largest reductions in SLP in the eddy-resolving SST run were associated with regions of deep atmospheric convection that warm the tropospheric column. These areas were shown to be related to the SST distribution with the greatest SLP reductions associated with convection over strong SST gradient regions. The landfall of a damaging convective meso-low on 8 June 2007 was also investigated. It was found that a region of strong SST gradients on the southern flank of a large warm ocean eddy was associated with lower SLP at the time of formation of this meso-low. In addition, the only case that simulated a meso-low at the correct time was the eddy resolved SST run. Based on this evidence it was hypothesized that the development of this meso-low was influenced by the eddy-scale SST distribution at the time, as well as the large-scale atmospheric conditions.

Model results for two ECL cases in 2007 (JUN07a and JUN07b) demonstrated that when a low pressure center lies over a warm eddy and has a similar spatial scale to the eddy, the effect of the ocean heat tends to increase the pressure gradient around the low pressure. The pressure gradient increases because of the pattern of areas increases in pressure over colder waters,

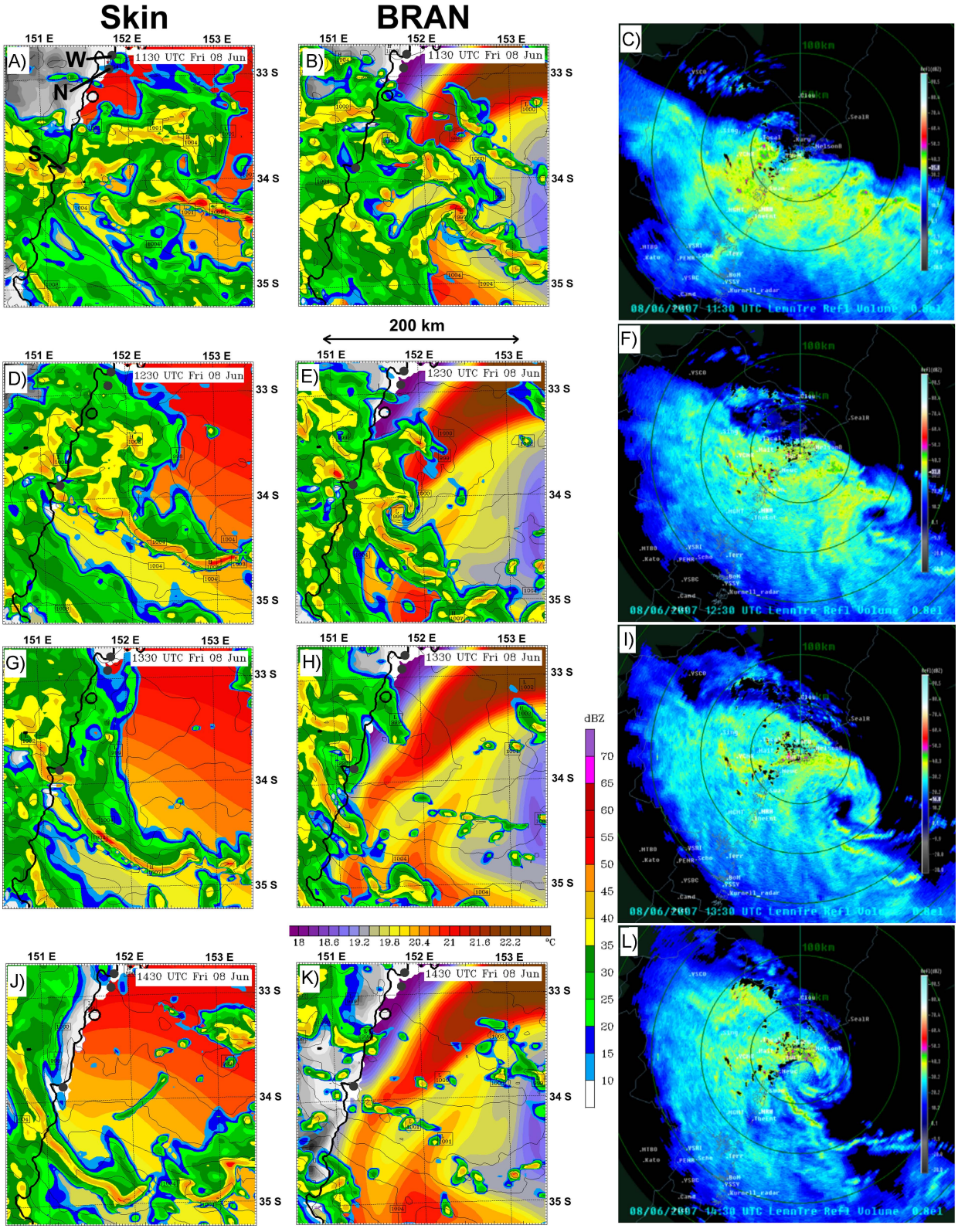

Figure 10: A comparison of hourly radar reflectivity (dBz) of the Skin (left panels), BRAN (middle) and observed (right, adapted from Mills *et al*., 2010) for the period from 1130 UTC (top row) to 1430 UTC (bottom row) 8 June 2007. The observed radar region was centered slightly north on Williamtown [indicated in the model plot region by the "W" in plot A) (also N is Nobbys and S is Sydney)]. The sea surface temperature (background over ocean colors, °C) and sea level pressure (black contours , hPa) were also plotted on the model plots.

surrounding an area of decreases in pressure over warmer waters. In this situation, the effect of SST distribution should be to strengthen the cyclonic flow around a low pressure. On the 48-hour time-scale the pressure gradient around the low pressure in the BRAN case was 0.5 to 1.5 hPa per 100 km greater than in the Skin case. The effect of this varied considerably over the inner model domain. The variability likely came from many factors: Horizontal heat advection could displace the SLP response downwind, SST induced cloud formation could increase the SLP response through enhanced atmospheric warming from latent heating, and slight displacement of a storm center that already contained a strong pressure gradient can cause a larger SLP difference (as exemplified in the two ECL cases in 2012).

The model results from the JUN07a case (7-9 June 2007) warranted further discussions because of the damaging coastal impacts that occurred as a result of this storm. It should be highlighted that coastal impacts were much localized around the Newcastle area despite the broad low pressure system. Given the presence of a large warm eddy just offshore at the time, a question arises; did the warm eddy contribute to the severity and localization of the coastal impacts? Chambers *et al*. (2014) found that the southern edge of the warm eddy was associated with an increase in rainfall. In the SLP response, we saw a reduction in SLP in regions and times that matched the rainfall changes. This occurred because rainfall increment were associated with increment of latent heating and consequently causing greater overall tropospheric warming, which resulting in the lowering of SLP. This type of SLP response can be a short time-scale response which is more relevant to convective scales. The lowering of SLP was the greatest over the SST gradient on the southern flank of the warm eddy as the convective band moved over the region indicating that the SST gradient can have a greater impact when an existing convective system passes over it.

The two ECL cases in 2012 (APR12 and JUN12) provided an interesting contrast to the 2007 cases. Part of this contrast was due to the fact that the 2012 cases were more rapidly developing and moving extra-tropical cyclones. The model generated a lower minimum 48-hourly time-mean SLP over the inner model domain in the Skin simulation (APR12_skin) than in the Bluelink simulation (APR12_OM). However, it was the Bluelink simulation that had a consistently lower minimum SLP over the inner model domain. This was because a dipole in SST developed as such that a region of lower pressure developed in the Bluelink simulation over the storm center, and higher pressure developed to the southeast of the center. What occurred was that the Bluelink simulation developed a tighter circulation with a slightly lower central pressure. This was evidenced that changing the SST caused noticeable structural changes to the extra-tropical cyclone as a whole that were not seen in the other cases. A very important note to make was that the change in the SST here only occurred for the 60 hours of the simulation and prior to that it was the same. Thus our analysis was concerned only with the immediate and short-term response to changes in the SST. Clearly, the specification of high-resolution of SST had the potential to greatly change and amplify the behavior of storms on time scales longer than a few days.

In conclusion the main findings of this investigation were:

- On the 48-hour time-scale covering the period of development and maturation of four ECLs, the introduction of eddy-resolving SSTs produced a general tendency to increase the SLP over cooler waters and lower the SLP over warmer waters.
- There were noticeable exceptions to this relationship and the 24-hour analysis indicated that the exceptions became greater in the second 24-hour period. This was associated with the propagation and in some cases amplification of changes seen in the first 24-hour period.
- The differences in SLP became greater as the time-scale of the analysis shortened, while at the same time the relationship with the SST became less clear. While this could be ascribed to be associated with chaotic amplification of small initial changes, an analysis of the evolution precisely showed that the amplified regions were related to SST differences at an earlier time.
- The greatest SLP changes tended to occur in the vicinity of either the low pressure center (APR12 and JUN12) or a severe convective line (JUN07a).
- The JUN07a_BN simulation suggested that the land falling severe mesoscale convective low pressure system observed on 8 June 2007 could have been directly triggered by the SST gradient on the southern flank of the large warm eddy present. The results from this case were very indicative, and fu-

ture work would look into the effect of strong SST gradients in similar storms to determine its effects on intense convective systems.

Conflict of Interest

No conflict of interest was reported by all authors.

Acknowledgements and Funding

The authors wish to thank the Lloyd's Register Foundation (LRF) who was the primary funder of this research. The LRF helps to protect life and property by supporting engineering-related education, public engagement and the application of research.

References

Bridgeman H A. (1986). The Sygna storm at Newcastle-12 years later. *Meteorology Australia*, 3(5), 10–16.

Browning K A and Landry C R. (1962). *Airflow Within a Tornadic Storm*. Preprints Tenth Weather Radar Conference. Washington DC, American Meteorological Society, 116–122.

Chambers C R S, Brassington G B, Simmonds I, *et al*. (2014). Precipitation changes due to the introduction of eddy-resolved sea surface temperatures into simulations of the "Pasha Bulker" Australian east coast low of June 2007. *Meteorology and Atmospheric Physics*, 125(1–2): 1–15. http://dx.doi.org/10.1007/s00703-014-0318-4.

Charney J and Eliassen A. (1964). On the growth of the hurricane depression. *Journal of the Atmospheric Sciences*, 21(1): 68–75. http://dx.doi.org/10.1175/1520-0469(1964)021<0068:OTGOTH>2.0.CO;2.

Cione J J, Raman S and Pietrafesa L J. (1993). The effect of Gulf Stream-induced baroclinicity on the U.S. East Coast winter cyclones. *Monthly Weather Review*, 121(2): 421–430. http://dx.doi.org/10.1175/1520-0493(1993)121<0421:TEOGSI>2.0.CO;2.

Dudhia J. (1989). Numerical study of convection observed during the Winter Monsoon Experiment using a mesoscale two-dimensional model. *Journal of Atmospheric Sciences*, 46(20): 3077–3107. http://dx.doi.org/10.1175/1520-0469(1989)046<3077:NSOCOD>2.0.CO;2.

Emanuel K A. (1986). An air-sea interaction theory for tropical cyclones. Part I: Steady-state maintenance. *Journal of the Atmospheric Sciences*, 43(6): 585–605. http://dx.doi.org/10.1175/1520-0469(1986)043<0585:AASITF>2.0.CO;2.

Emanuel K A. (1988). The maximum intensity of hurricanes. *Journal of the Atmospheric Sciences*, 45(7): 1143–1155. http://dx.doi.org/10.1175/1520-0469(1988)045<1143:TMIOH>2.0.CO;2.

Giordani H, Caniaux G. (2001). Sensitivity of cyclogenesis to sea surface temperature in the northwestern Atlantic. *Monthly Weather Review*, 129(6): 1273–1295. http://dx.doi.org/10.1175/1520-0493(2001)129<1273:SOCTSS>2.0.CO;2.

Global Climate and Weather Modeling Branch. (2003). The GFS atmospheric model. *NCEP Office Note 442*.

Griffies S M, Harrison M J, Pacanowski R C. (2008). A Technical Guide to MOM4. *GFDL Ocean Group Technical Report NO. 5*.

Hamon B V. (1965). The East Australian Current, 1960-1964. *Deep-Sea Research*, 12(6): 899–921. http://dx.doi.org/10.1016/0011-7471(65)90813-2.

Hendricks E A, Montgomery M T and Davis C A. (2004). The role of "vortical"hot towers in the formation of tropical cyclone Diana (1984). *Journal of the Atmospheric Sciences*, 61(11): 1209–1232. http://dx.doi.org/10.1175/1520-0469(2004)061<1209:TROVHT>2.0.CO;2.

Holland G J, Lynch A H and Leslie M L. (1987). Australian east-coast cyclones. Part 1: Synoptic overview and case study. *Monthly Weather Review*, 115(12): 3024–3036. http://dx.doi.org/10.1175/1520-0493(1987)115<3024:AECCPI>2.0.CO;2.

Hong S Y, Noh Y and Dudhia J. (2006). A new vertical diffusion package with an explicit treatment of entrainment processes. *Monthly Weather Review*, 134(9): 2318–2341. http://dx.doi.org/10.1175/MWR3199.1.

Jacobs N A, Lackmann G M and Raman S. (2005). The combined effects of Gulf Stream-induced baroclinicity and upper-level vorticity on US east coast extratropical cyclogenesis. *Monthly Weather Review*, 133(8): 2494–2501. http://dx.doi.org/10.1175/MWR2969.1.

Jacobs N A, Raman S, Lackmann G M, *et al*. (2008). The influence of the Gulf Stream induced SST gradients on the US East Coast winter storm of 24–25 January 2000. *International Journal of Remote Sensing*, 29(21): 6145–6174. http://dx.doi.org/10.1080/01431160802175561.

Janjic Z I. (1994). The step-mountain eta coordinate model: Further developments of the convection, viscous sublayer, and turbulence closure schemes. *Monthly Weather Review*, 122(5): 927–945. http://dx.doi.org/10.1175/1520-0493(1994)122<0927:TSMECM>2.0.CO;2.

Kuwano-Yoshida A, Minobe S and Xie S P. (2010). Precipitation response to the Gulf Stream in an atmospheric GCM. *Journal of Climate*, 23(13): 3676–3698. http://dx.doi.org/10.1175/2010JCLI3261.1.

McInnes K L, Leslie L M and McBride J L. (1992). Numerical simulation of cut-off lows on the Australian east coast: Sensitivity to sea-surface temperature. *International Journal of Climatology*, 12(8): 783–795.

http://dx.doi.org/10.1002/joc.3370120803.

Lim E P and Simmonds I. (2002). Explosive cyclone development in the Southern Hemisphere and a comparison with Northern Hemisphere events. *Monthly Weather Review*, 130(9): 2188–2209. http://dx.doi.org/10.1175/1520-0493(2002)130<2188:ECDITS>2.0.CO;2.

Miller B I. (1958). On the maximum intensity of hurricanes. *Journal of Meteorology*, 15(2): 184–185. http://dx.doi.org/10.1175/1520-0469(1958)015<0184:OTMIOH>2.0.CO;2.

Mills G A, Webb R, Davidson N *et al*. (2010). The Pasha Bulker east coast low of 8 June 2007. *CAWCR technical report NO. 23*.

Mlawer E J, Taubman S J, Brown P D, *et al*. (1997). Radiative transfer for inhomogeneous atmosphere: RRTM, a validated correlated-k model for the longwave. *Journal of Geophysical Research*, 102 (D14): 16663–16682. http://dx.doi.org/10.1029/97JD00237.

O'Neill L W, Chelton D B and Esbensen S K. (2010a). The effects of SST-induced surface wind speed and direction gradients on midlatitude surface vorticity and divergence. *Journal of Climate*, 23(2): 255–281. http://dx.doi.org/10.1175/2009JCLI2613.1.

O'Neill L W, Esbensen S K, Thum N, *et al.* (2010b). Dynamical analysis of the boundary layer and surface wind responses to mesoscale SST perturbations. *Journal of Climate*, 23(3): 559–581. http://dx.doi.org/10.1175/2009JCLI2662.1.

Oke P R, Brassington G B, Griffin D A, *et al.* (2008). The Bluelink ocean data assimilation system (BODAS). *Ocean Modelling*, 21(1–2): 46–70. http://10.1016/j.ocemod.2007.11.002.

Park K A, Cornillon P and Codiga D L. (2006). Modification of surface winds near ocean fronts: Effects of Gulf Stream rings on scatterometer (QuikSCAT, NSCAT) wind observations. *Journal of Geophysical Research*, 111(C3): C03021. http://dx.doi.org/10.1029/2005JC003016.

Pepler A S, Di Luca A, Ji F, *et al.* (2015). Impact of identification method on the inferred characteristics and variability of Australian East Coast Lows, *Monthly Weather Review*, 143(3): 864–877. http://dx.doi.org/10.1175/MWR-D-14-00188.1.

Persing J and Montgomery M T. (2003). Hurricane superintensity. *Journal of the Atmospheric Sciences*, 60(19): 2349–2371. http://dx.doi.org/10.1175/1520-0469(2003)060<2349:HS>2.0.CO;2.

Pope C. (1968). Winter cyclogenesis with tropical characteristics over the Gulf Stream. *Monthly Weather Review*, 96(12): 867–875. http://dx.doi.org/10.1175/1520-0493(1968)096<0867:WCWTCO>2.0.CO;2.

Roebber P J. (1984). Statistical analysis and updated climatology of explosive cyclones. *Monthly Weather Review*, 112(8): 1577–1589. http://dx.doi.org/10.1175/1520-0493(1984)112<1577:SAAUCO>2.0.CO;2.

Sanders F and Gyakum J R. (1980). Synoptic-dynamic climatology of the "bomb". *Monthly Weather Review*, 108(10): 1589–1606. http://dx.doi.org/10.1175/1520-0493(1980)108<1589:SDCOT>2.0.CO;2.

Schiller A, Oke P R, Brassington G B, *et al*. (2008). Eddy-resolving ocean circulation in the Asian-Australian region inferred from an ocean reanalysis effort. *Progress in Oceanography*, 76 (3), 334–365. http://dx.doi.org/10.1016/j.pocean.2008.01.003.

Skamarock W C, Klemp J B, Dudhia J, *et al.* (2005). A description of the Advanced Research WRF Version 2. *NCAR Technical Note*, 468.

Small T J, deSzoeke S P, Xie S P, *et al.* (2008). Air–sea interaction over ocean fronts and eddies. *Dynamics of Atmospheres and Oceans*, 45(3–4), 274–319. http://dx.doi.org/ 10.1016/j.dynatmoce.2008.01.001.

Thompson G, Rasmussen R M and Manning K. (2004). Explicit forecasts of winter precipitation using an improved bulk microphysics scheme. Part I: Description and sensitivity analysis. *Monthly Weather Review*, 132(2): 519–542. http://dx.doi.org/10.1175/1520-0493(2004)132<0519:EFOWPU>2.0.CO;2.